This is the accepted manuscript made available via CHORUS. The article has been published as:

Effects of reactive elements on the structure and diffusivity of liquid chromia: An ab initio molecular dynamics study

H. Z. Fang, W. Y. Wang, Paul D. Jablonski, and Z. K. Liu

Phys. Rev. B **85**, 014207 — Published 30 January 2012

DOI: 10.1103/PhysRevB.85.014207

Effects of reactive elements on the structure and diffusivity of liquid chromia: an *ab-initio* molecular dynamics study

H. Z. Fang [1], W. Y. Wang [1], Paul D. Jablonski [2] and Z. K. Liu [1]

[1] *Department of Materials Science and Engineering, The Pennsylvania State University, University Park, PA 16802, USA*

[2] *National Energy Technology Laboratory, Department of Energy, Albany, OR 97321, USA*

Abstract

Effects of minor addition of reactive elements (Ce, Hf, La, Y and Zr) on the structural and dynamical properties of liquid chromia were investigated by the ab-initio molecular dynamics approach. The calculation results show that minor doping of reactive elements has a significant effect on the diffusivity of chromium and oxygen ions. It is observed that Hf and La are the most efficient elements in retarding the diffusion of chromium and oxygen, Ce and Y are the secondarily efficient, while Zr is the least efficient. The relative bonding strength between doping elements and oxygen was found to be in descending order of Hf-O>Zr-O>(Ce,Y)-O>La-O, which could be estimated from the major peak intensity of pair correlation functions or the value of mean residence time. Our calculation results are in satisfactory agreement with those obtained from experimental measurement and thermodynamical database. The mechanism regarding the effects of reactive element on diffusivity was further analyzed in view of possible factors: ionic size, bonding strength, and ionic weight. It turns out no sole factor could be responsible for the relative efficiency of reactive elements, and a novel evaluation parameter combining these factors was proposed.

PACS number(s): 66.10.cg, 61.20.Ja, 47.11.Mn, 31.15.A-

1. Introduction

The Cr_2O_3 scale provides great protection against the oxidation of a variety of Cr-containing alloys from low temperatures up to about 700 ℃, such as the Fe-Cr based stainless steels and the Ni-Cr based superalloys. However, at temperatures above 700 ℃ the vaporization of Cr and spallation of Cr_2O_3 scale take place and reduce its protectiveness [1-3]. It has been demonstrated through extensive experiments [2-10] that the addition of a minor amount of reactive elements (REs) such as Ce, Y, La, etc. often leads to a significant improvements of the oxidation resistance of the base alloy at elevated temperatures, which was termed as the "reactive element effect" [5-6, 9]. The reactive element effect has been widely applied to industrial applications under high temperature conditions, for example, the interconnect for solid oxide fuel cells and the bond coating system for turbine blades. Several mechanisms have been postulated in the literature [5-7]. These include a finer oxide morphology, an improved scale-metal interface and a modification of oxidation kinetics. About two decades ago, Stringer et al [5] assumed to a first approximation that the effect of different REs appears to be the same. However, recent studies, such as those conducted by Ramanathan et al [2] and Fontana et al [10], indicate that this effect is not universal, but depend on the nature of both reactive elements and base alloys. To date, the mechanisms through which the reactive element effects are produced are not yet fully understood [8-9] and the optimization of REs addition has still been a matter of trial and error. The primary goal of the current work is to evaluate the relative efficiency of different REs on slowing the diffusion process within the chromia scale.

It has been widely accepted that the oxidation kinetics cannot be explained by bulk diffusion as the main mode of transport, rather they are probably controlled by grain boundary diffusion [11-14]. The diffusivities of chromium and oxygen in the grain boundary are measured to be 10^3~10^6 times higher than those in the bulk lattice [13]. Meanwhile, the doped REs have been observed to segregate into the grain boundary [2-3, 5, 11]. Experimental observations [3, 6-7, 10] reveal that the doping of REs changes the diffusion mechanism during the chromia scale formation from outward diffusion of chromium ions to inward diffusion of the oxygen ions. However, the relative efficiency of different REs in this process has not yet been analyzed and classified in depth, and theoretical studies are still not sufficient.

In the present work, the effects of a select group of reactive elements on the diffusivity and atomic-scale structure of liquid Cr_2O_3 were studied by the ab-initio molecular dynamics (AIMD) approach. There are several considerations that motivate us to choose liquid state Cr_2O_3 as the research prototype rather than a certain type of grain boundary of polycrystalline Cr_2O_3. One is that the structure of an actual grain boundary is so complex that it cannot simply be represented by a single type of grain boundary model, such as the one based on the concept of coincident site lattice. It has been reported on various systems, including semiconductors, metals, and ceramics (such as aluminum oxide, zinc oxide, silicon nitride and etc.), at high temperature, the nano-scale grain boundary complexion with high interfacial energy becomes disordered and exhibits a universal, highly confined, liquid-like structure, as evidenced by both experimental and theoretical studies [15-18]. Thus the structure of a high-temperature grain boundary could be considered to be closely related to a supercooled liquid, in which the diffusion mechanism is analogous to that in the liquid state. Another consideration is that the state-of-art AIMD technique has been demonstrated to be powerful and straightforward to reveal the structural and transport properties of liquid phases [19-23], which calculates interatomic forces on-the-fly based on the density functional theory (DFT) and does not require a priori knowledge of an empirical model potential, which is a critical problem for classical molecular dynamics simulation.

2. Computational methods

The AIMD calculations in this work are performed by employing the Vienna ab initio simulation package (VASP) [24-25] of the latest version (V5.2). The first-principles calculations presented here are based on DFT with the ion-electron interaction described by the projector augmented wave [26] method and the electronic exchange correlation interaction by the generalized gradient approximation parameterized by Perdew and Wang [27]. The valence electrons considered in the pseudopotentials for each atomic species are as follows: $2s^2 2p^4$ for O, $3d^5 4s^1$ for Cr, $4f^1 5d^1 6s^2$ for Ce, $5d^3 6s^1$ for Hf, $5s^2 5p^6 5d^1 6s^2$ for La, $4s^2 4p^6 4d^2 5s^1$ for Y and $4d^3 5s^1$ for Zr. Newton's equation of motion is solved via the Verlet algorithm with a timestep of 3 fs. The simulations are performed in a canonical ensemble (NVT) with a Nosé thermostat for temperature control [28]. Two precision schemes are introduced in our AIMD calculations: one is the high precision scheme for calculating exact external pressure in a short run and the other is the low precision scheme for a long production calculation run. Within the low precision scheme, we use only Γ point to sample the Brillouin zone and an energy of 300 eV to cut off the plane wave basis. Within the high precision scheme, we adopt a denser 2×2×2 K-points generated by the Monkhorst-Pack [29] method and a higher cutoff energy of 520 eV. The timestep and the thermostat are carefully chosen so that a small total energy drift (<10 meV/atom/ps) is maintained during the equilibrium run.

The simulated cubic supercells are initially constructed with all atoms randomly distributed according to the stoichiometry: *i.e.*, 40 Cr and 60 O atoms for pure chromia, 40 Cr, 60 O and 1 RE (RE = Ce, Hf, La, Y, Zr) atoms for RE-doped systems, similar to our previous work [19-21]. The volumes of the initial supercells are set according to an atomic-number density of 0.09218 atoms/Å^3, which is extrapolated from the density and thermal expansion coefficient of the rhombohedral α-Cr_2O_3 [30]. We perform AIMD calculations at three different temperatures: 4000 K, 3300 K and 2705 K (melting point of α-Cr_2O_3). To obtain a more accurate density of the liquid state, the supercell volume at each temperature is adjusted according to the condition of zero external pressure [19-23], and the detailed procedures are as follows: firstly, the initial configuration is relaxed for 2000 MD steps within the low precision scheme; secondly, we apply several small isotropic volume strains to the last configuration obtained above, and then run 300~500 MD steps in the high precision scheme for each supercell with a volume strain to derive the exact external pressure; thirdly, the pressure-volume data are fitted by a quadratic polynomial and the volume corresponding to zero pressure is taken as the equilibrium volume at that temperature. A long production run is finally carried out for 18 ps within the low precision scheme for the configuration with the adjusted volume obtained from the above calculation. During the intermediate stage, a cooling rate of 6.7×10^{13} K/s is used to cool the liquid from the higher temperature to the lower one. Six thousand configurations are collected at each temperature, the first five hundred ones are removed when analyzing the diffusion properties, and the last two hundred ones are used for structural analysis.

3. Results and discussions

3.1 Structural properties

In a molecular dynamics simulation, the pair correlation function and the bond pair analysis technique serve as two important tools to gain insight into the structural disorder and structural evolution of the liquid state.

3.1.1 Pair correlation function

The pair correlation function is defined as the probability of finding one atom at the radius of r when taking another atom as the center compared to a homogeneous distribution and is given by the following [31-32],

$$g_{AB}(r) = \frac{V}{N_A N_B}\left\langle \sum_{i=1}^{N_A} n_{iB}(r,\Delta r) \Big/ 4\pi r^2 \Delta r \right\rangle \tag{1}$$

In the above equation, V is the volume of the simulation supercell, N_A and N_B are the numbers of A and B atoms, respectively, and n_{iB} represents the number of B atoms found in a shell from r to $r+\Delta r$ whose center is atom i.

The partial pair correlation function curves of Cr-Cr, O-O, Cr-O and RE-O pairs for the pure and RE-doped chromia systems at the three investigated temperatures are shown in FIG. 1 (a)-(d). The label "-RE" (RE = Ce, Hf, La, Y or Zr) in FIG. 1 denotes the chromia system doped by this species of RE, and henceforth. It can be seen that all the pair correlation function curves in FIG. 1 (a)-(c) exhibit two considerable broad peaks at a short distance superimposed on an oscillatory trace to 1.0, which is a characteristic of a liquid system, indicating the geometrical short range order of atomic arrangement. FIG. 1 (d) shows some noise signals imposed on the two major peaks, which is due to the minor addition of dopants (~1% atomic basis), but these noise signals are not strong enough to affect our qualitative analysis of the intensities of the first major peaks.

From FIG. 1 (a)-(c), it can be seen that the profiles of pair correlation function curves for the Cr-Cr, O-O and Cr-O pairs with different dopants are very similar at the same temperature, which implies the minor doping of REs has not significantly changed the local geometrical structure of liquid chromia. By comparing the four pair correlation function curves of Cr-Cr, O-O, Cr-O and RE-O pairs at the same temperature, such as at 4000 K, it can be found that the intensities of the first peaks of the homogeneous pairs (Cr-Cr and O-O) are much weaker than the heterogeneous pairs (Cr-O and RE-O). This phenomenon indicates that there are strong chemical attractive interactions (or bonding strength) between Cr and O and between the doped RE and O, reflecting chemical short range order (CSRO) of atomic packing. From the RE-O pair correlation function curves at each of the three simulated temperatures (FIG. 1 (d)), it can be observed that the intensities of the first peaks are in the sequence of $I_{\mathrm{Hf\text{-}O}}>I_{\mathrm{Zr\text{-}O}}>I_{\mathrm{Ce\text{-}O}}(I_{\mathrm{Y\text{-}O}})>I_{\mathrm{La\text{-}O}}$ and this sequence is nearly independent of temperature. The first peak intensities for the Ce-O and Y-O pairs are very close to each other, so that their relative intensities in the sequence are not determinable. Since the position of the first peak is corresponding to the equilibrium bonding distance between ions, the intensity of the first peak is corresponding to the relative density of bonding ions and thus indicates the strength of bonding. Meanwhile, since the doping concentrations are the same for all the considered reactive elements, the chemical attraction (or relative bonding strength) between the RE ion and oxygen can be compared on the equivalent environment of liquid state. From FIG. 1, it can also be seen that as temperature decreases, the intensities of the first peaks of all pair correlation function curves increase, which implies the development of the degree of SRO in liquid structures.

Besides deriving the information of bonding strength from the first peak intensity of the pair correlation function curve, one can also obtain the bonding length from the position of the first peak and the partial coordination number from the integration of the first peak as follows,

$$N_{AB}(r)=\int_0^{r_{cut}} 4\pi r^2 \rho_B g_{AB}(r)dr \tag{2}$$

where r_{cut} is the cutoff distance defined by the first minimum position of $g_{AB}(r)$, and ρ_B the average atomic density of B. The average of the first minimum positions of $g_{AB}(r)$ of all the three temperatures is used to determine the cutoff distance. The calculated values are listed in Table along with the experimental coordination numbers of α-Cr_2O_3 with rhomohedral structure taken from Belokoneva et al [33].

Table shows that the bonding length of the O-O pair in the liquid state is larger than that in the crystal state, while the bonding length of the Cr-O pair in the liquid state is much smaller than that in the crystal state. This means that due to the less dense packing of the liquid state, the negatively charged O ions have more freedom to repel each other to a longer distance, and the Cr and O ions with opposite charges could attract each other to a shorter distance. From Table , it can also be seen that there are two r_{max} values for the Cr-Cr pair, which corresponds to the two subpeaks imposed on the first broad peak of Cr-Cr pair correlation function curve (FIG. 1a). These two subpeaks are related to the first neighbor (2.89 Å) and the second nearest neighbor (3.42 Å) among the Cr ions, similar to those in α-Cr_2O_3, reflecting the structural associations between liquid and crystal states. The bonding length between REs and oxygen is found in the same sequence as the cationic radii, which are 0.71, 0.72, 0.87, 0.9 and 1.032 Å for the Hf^{4+}, Zr^{4+}, Ce^{4+}, Y^{3+} and La^{3+} ions, respectively, based on Shannon's table [34] with an identical coordination number value of six. Such an agreement shows the validity of our AIMD simulations. The partial coordination numbers of Cr-Cr, O-O and Cr-O pairs have a tendency of increasing as the temperature decreases in the liquid state, but they are smaller than those in the crystal state within the same cutoff distance, indicating the local structure in the liquid state is less densely packed than that in the crystal state.

3.1.2 Bond pair analysis

To gain more insight into the structural features of the liquid state, the bond pair analysis technique proposed by Honeycutt and Anderson [35] is utilized. Four index numbers *i*, *j*, *l*, *m* are used to distinguish the geometrical short range order surrounding each atom. Two atoms form a bond when they are within a cutoff distance, which corresponds to the distance to the first minimum of the pair correlation function curve in our analysis. If atom A and atom B form a bond, $i = 1$ and otherwise $i = 2$. j denotes the number of common neighbors which form bonds with both atom A and atom B. l represents the number of bonds formed between the common neighboring atoms. m is used to distinguish clusters with the same first three indices but with a different topology.

In FIG. 2, we show the five most frequent bond pair types found in the structure of the liquid chromia. The proportion of 15*lm* type bond pairs is a sum of bond pairs whose first two indices are the same (like 1541, 1551, 1552, 1561 …), and likewise for the 13*lm*, 14*lm*, 16*lm*, 17*lm* type bond pairs. From Fig. 2, it can be seen that the 15*lm* type bond pairs, which are the characteristic bond pair of five-fold symmetric clusters (such as the icosahedra), dominate in the liquid state, as has been extensively reported in literatures [19-23]. The existence of full or defect icosahedral clusters in the liquid state results from the requirement of efficient packing of ions. As it can be seen, the proportion of 15*lm* type bond pairs increases gradually as temperature decreases. The 14*lm* and 16*lm* type are the next most frequent bond pairs in liquid chromia. In α-Cr_2O_3, one chromium ion forms bonds with six neighboring oxygen ions, and one oxygen ion forms bonds with four chromium ions. The 14*lm* and 16*lm* type bond pairs are a reflection of similarities between the liquid structure and the corresponding crystal structure, and the mixture of 15*lm,* 14*lm,* and 16*lm* give further validity to using liquid Cr_2O_3 to represent the disordered grain boundary structure. The low proportion of 13*lm* and 17*lm* type bond pairs reflects various disordered clusters existing in the liquid chromia. Comparing with the pure and RE-doped systems (here we only show the case of Hf for clarity), one can see the distribution of bond pairs are very similar, indicating that the doping of REs has not changed the liquid structure remarkably, which is consistent with the analyses from the pair correlation function curves above.

3.2 Dynamical properties

The self diffusion coefficient of atoms in liquid could be derived from the mean square displacement (MSD) based on Einstein's relation or from the velocity autocorrelation function (VACF) based on Green-Kubo relation [31-32].

The time-dependent mean square displacement for A atoms is defined as

$$\left\langle \Delta r_A(t)^2 \right\rangle = \frac{1}{N_A} \left\langle \sum_{i=1}^{N_A} \left| \vec{r}_{Ai}(t+t_0) - \vec{r}_{Ai}(t_0) \right|^2 \right\rangle \tag{3}$$

where the sum goes over all A atoms, t_0 is an arbitrary time origin and the angular brackets denote a thermal average or equivalently an average over time. According to Einstein's relation, the mean square displacement is linear in t for random walk of atoms and the slope is proportional to the diffusion coefficient D_A of atom A:

$$\left\langle \Delta r_A(t)^2 \right\rangle \to 6D_A t + C_A \tag{4}$$

where C_A is constant. A linear fitting of least square regression is performed on the mean square displacement curve to obtain the diffusivity.

The mean square displacement curves of Cr and O ions at 2705 K in the pure and RE-doped liquid chromia are shown in FIG. 3. The mean square displacement at the other two simulated temperatures are similar and not included in the paper. From FIG. 3, one can see that at 9 ps, the mean square displacements of Cr ions reach 50~70 Å^2, while those of O ions reach 60~80 Å^2, both large enough compared to the ionic radius for obtaining good statistics of the trajectories of motion. The calculated self diffusivities of Cr and O elements at the three investigated temperatures are listed in Table . For comparison of the accuracy of the calculated results, Table also lists the diffusivity data derived from the velocity autocorrelation function based on Green-Kubo relation, which is defined as

$$D_A = \frac{1}{3N_A}\int_0^{\infty}\left\langle \sum_{i=1}^{N_A} \vec{V}_{Ai}(t+t_0)\cdot \vec{V}_{Ai}(t_0)\right\rangle dt \tag{5}$$

and the normalized velocity autocorrelation function is given by,

$$\psi_A(t) = \frac{\left\langle \vec{V}_{Ai}(t+t_0)\cdot \vec{V}_{Ai}(t_0)\right\rangle}{\left\langle \vec{V}_{Ai}(t_0)\cdot \vec{V}_{Ai}(t_0)\right\rangle} \tag{6}$$

where $\vec{V}_{Ai}(t)$ is the velocity of the i^{th} atom, t_0 and the angular bracket have been noted before. FIG. 4 shows the normalized velocity autocorrelation function curves of Cr and O ions at 2705 K in the pure and Hf-doped liquid systems. As one can see, there are two oscillations on the asymptotic curves of O ions in both systems, indicating the frequent collisions between O atoms. However, no obvious oscillation on the curves of Cr can be observed, indicating that much less collisions occur between Cr atoms. This also implies that Cr ions are preferably surrounded by the oppositely charged O ions, consistent with the structural analysis in the section above. Table indicates that the self diffusivities derived from the mean square displacement and velocity autocorrelation function methods are consistent with each other. For both methods, the statistical errors (given in Table II) are estimated from the standard deviation defined by $\sigma = \sqrt{\sum_{t=1}^{N_t}(D(t)-\bar{D})^2/(N_t-1)}$, where N_t is the number of the discrete sampling time t, $\bar{D}$ is the average diffusivity. It can be seen that, in most cases the statistical errors are within 10%. One can also find out that the diffusivities of O are larger than those of Cr for both pure and RE-doped systems, which is in line with the results from tracer diffusion experiments using isotopes by Sabioni et al [36] and Park et al [37], although the temperatures studied in the current work are much higher than those in the experiments (1373 K~1723 K). The Arrhenius plots showing the temperature dependences of the diffusivities of O element in different systems are given in FIG. 5 (d). The diffusion activation energy for oxygen in the pure liquid chromia is estimated to be 53.6 kJ/mol, which is much smaller than the measured value of 419 kJ/mol in the solid state at the temperature range 1350 K to 1675 K [38], indicating the quite larger mobility of ions in liquid. Even though the linearities are not always satisfactory for all the considered systems, as shown in FIG. 5 (d), which might be caused by the statistical errors and limited diffusivity data points, it can be found out that the activation energy for oxygen diffusion does not vary considerably (<8%) with the minor addition of dopants.

In order to compare the effect of doping elements on diffusivity, the diffusivity ratios of $D_{\mathrm{Cr}}/D_{\mathrm{O}}$ in RE-doped chromia to that in pure chromia are plotted in FIG. 5 (a-c) for different temperatures. One can see that the diffusivities of both Cr and O are reduced remarkably through the doping of REs except for Zr. However, the sequences of the ability of REs to retard the diffusion seems not to be the same at different temperatures, such as for the efficiency to retard the diffusion of O, it is Hf >La>Y>Ce>Zr at 4000 K, while Hf>Ce>Y>La>Zr at 3300 K and La>Hf>Y>Ce>Zr at 2705 K. Such differences are probably resulting from the limited accuracy of the statistics in molecular dynamics calculations (around 10% in current work). Nevertheless, some general features could be observed regarding the effect of dopants: the Hf and La are the most efficient elements to retard the diffusion of Cr and O, the Ce and Y are the secondarily efficient ones while the Zr is the least efficient one. Experimentally, Ramanathan et al [2] reported that La is one of the most efficient element to improve the corrosion resistance of Fe-20Cr alloy, while Ce and Y have much less effect among the REs they studied, and they attributed the excellent efficiency of La to its large ionic radius. Fontana et al [10] found that a La_2O_3 coating has a much better effect than a Y_2O_3 coating for the three commercial alloys they studied: Crofer 22 APU, AL 453 and Haynes 230, which are used as the interconnects for solid oxide fuel cell. Especially for the AL 453 alloy, the thickness of the oxide scale decreases dramatically from 1040 nm when coated by Y_2O_3 to 490 nm when coated by La_2O_3, after 100 hours at 800 ℃ under atmospheric conditions. A recent experimental study [39] also demonstrated that Hf has a much better beneficial effect on the improvement of the oxidation resistance of a Ni-Al-Cr alloy than either Zr or Y.

4. Discussions

As mentioned in the first section, it has been reported that there are structural similarities between liquid and high-temperature grain boundaries, and therefore it is reasonable to assume that the diffusivity and the effects of reactive element in these two states are similar to some degree. In the following, the observed effects of doped REs on the diffusivity in liquid Cr_2O_3 will be discussed from the atomic scale, in terms of the ionic size, the bonding strength between cation and oxygen, and the ionic weight.

4.1 Ionic size and coordination number of doping elements

It is reported that the doping REs, such as La^{3+}, Y^{3+} and Ce^{4+}, with a larger ionic size than Cr^{3+} or Al^{3+} show a strong tendency to segregate into grain boundaries in Cr_2O_3 [2-3] or Al_2O_3 [39-41]. It is commonly accepted that these larger RE ions block or impede the movement of Cr or Al along the grain boundaries in Cr_2O_3 or Al_2O_3 scales, respectively, and reduce the growth rate of oxide scales, which is commonly referred as “site-blocking” effect [41]. Ramanathan et al [2] observed a direct correlation between ionic radius of RE and oxidation residence for RE oxide coated Fe-20Cr alloy. For our simulations in liquid, the La^{3+} has the largest radius among the investigated RE ions, estimated from the positions of the first peaks of RE-O pair correlation function curves. It is important to note that La^{3+} can incorporate more O^{2-} in the nearest neighboring shell shown by the largest coordination number, 9.6~10.6 in Table . Thus La forms more bonds with O and reduces the accessibility of Cr to O. By the same token, Y^{3+} and Ce^{4+} are more efficient on blocking Cr from O than Zr^{4+}. However, FIG. 5 shows the doping of Hf has more significant effect on the diffusivities than the doping of Ce and Y, even though the ionic size of Hf^{4+} is smaller than Ce^{4+} or Y^{3+}. Therefore, the ionic size is not the sole factor in determining the effect of reactive element on diffusivities of ions.

4.2 Bonding strength between cation and oxygen

Both the diffusion along grain boundaries and in liquid states involves the breaking of bonds between cations and oxygen, and thus the bonding strength could be a very important factor for considering the effects of reactive elements. In the current AIMD simulations, the bonding strength could be evaluated from the first peak intensity of the RE-O pair correlation function curves and a statistical value of mean residence time. The latter was calculated from the average time for which the oxygen ions reside in the first neighboring range of cations, as shown in FIG. 6.

It can be seen from FIG. 1 (d) and FIG. 6 (b) that both the pair correlation function and mean residence time methods indicate similar sequence of bonding strength as Hf-O>Zr-O>(Ce,Y)-O>La-O. Again the relative bonding strength between Ce-O and Y-O cannot be differentiated. Furthermore, bonding strength may also be characterized in terms of melting temperature T_m, enthalpy of formation ΔH_f and enthalpy of melting ΔH_m calculated from the

SGTE database [42] as listed in Table III. As discussed by Kim et al. [39], in general, the higher values of T_m and ΔH_m indicate the stronger bonding between cation and oxygen. From Table III, one can see that the sequence of bonding strength between RE and oxygen estimated from our molecular dynamics simulations is consistent with that estimated from ΔH_f, though ZrO_2 and Cr_2O_3 break the sequence in terms of T_m, and La_2O_3 breaks the sequence in terms of ΔH_m. Since the bonding between Hf^{4+} and O^{2-} is the strongest judging from the pair correlation function, mean residence time, T_m, ΔH_f, and ΔH_m, Hf is thus shown to be one of the most efficient elements in retarding the diffusion of O, as seen in FIG. 5. Since the diffusion of Cr requires the breaking of RE-O bonds, the stronger RE-O bonding thus slows down the migration of Cr. The bonds between Ce^{4+} and O^{2-} and between Y^{3+} and O^{2-} are also relatively strong, indicating their efficiency in retarding the diffusion of ions in liquid Cr_2O_3. However, even though Zr has the bonding strength with oxygen nearly equal to that of Hf, it is the least efficient element in reducing the diffusivities of oxygen, while the La with the weakest bonding strength with oxygen is one of the most efficient elements, indicating that there are more factors that need to be considered in evaluating the effects of reactive elements.

4.3 Ionic weight of doping elements

Under the same driving force, Newton's equation of motion indicates that lighter atoms move faster than heavier atoms. Usually, the weight of diffusing particles is implicitly involved in the diffusion equation. Experimental and theorectical studies [43-45] have revealed an inverse dependence of the diffusivity D on the mass M of diffusing particles in liquid metals as $D \propto M^{-1/2}$. Table III shows that the Hf^{4+} has the largest ionic weight, whereas the ionic weight of Zr^{4+} is just 66% of that of La^{3+} and 51% of that of Hf^{4+}. Therefore the lighter Zr^{4+} moves faster than Hf^{4+}

and La^{3+}, as also been demonstrated by the curves of mean square displacement vs. time of Zr^{4+} which are highly above those of La^{3+} and Hf^{4+} at each temperature (not shown here). From the structure analysis of the liquid RE-doped Cr_2O_3, we know that the doped RE ions are located in atomic clusters which contain O as the major species and Cr as a minor species. Consequently, the faster moving Zr^{4+} can bring the surrounding O^{2-} to move faster with contribution from the strong bonding between them.

4.4 Combined contributions from more than one factors

The analyses above indicate that usual suspects of factors of doping elements, i.e. ionic size and coordination number, bonding strength between cation and oxygen, and ionic weight, individually cannot account for the effect of doping elements on the diffusivity of constituent ions, which is probably due to the fact that some factors are not independent but correlated with each other. The bonding strength was first defined by Pauling [46] as the valence of cation Z divided by its coordination number N: $S=Z/N$. Through extensive studies of Brown et al. [47] and Ziolkowski [48], the bond strength S was found in inverse relation to the bond length R (or ionic radius), typically in the empirical relation $S=S_0(R/R_0)^{-m}$, where the parameter S_0 is assigned arbitrarily by the user and R_0 and m (=2~6) are fitting constants. In current work, we combine the above two relations and evaluate the relative bonding strength of RE-O as,

$$S = C\frac{Z}{NR^m} \tag{7}$$

Where, C is a constant, the bonding strength S could be represented by the mean residence time or the first peak intensity of pair correlation function, and coordination numbers N are the number of oxygen ions in the first neighboring shell of respective reactive elements, as shown in Table . A good linear relationship between the bonding strength and the term on the right hand side of Equation 7 is observed when m=2, as shown in FIG. 7. This excellent agreement between our AIMD calculations and the empirical relations derived from extensive experimental data demonstrates not only the accuracy of current AIMD calculations, but also the validity of our former statement that both the mean residence time and the first peak intensity of pair correlation function can represent the bonding strength of RE and oxygen. From Equation 7, it can be deduced that the ionic size (or coordination number) and the bonding strength are in the inverse relation and must exhibit a competing influence on the efficiency of reactive element to retard the diffusion of constituent ions.

On the other hand, how to combine various factors to understand the effects of reactive element is a long-standing open issue [5, 8]. Based on the above analysis, we attempt to bring forward an effective parameter ε to combined the factors discussed in current work as,

$$\varepsilon = \left(\frac{R_{RE}}{R_{Cr}}\right)^2 \frac{S_{RE\text{-}O}}{S_{Cr\text{-}O}} \left(\frac{M_{RE}}{M_{Cr}}\right)^{1/2} \tag{8}$$

To demonstrate the validity of this parameter, we show the diffusivities of oxygen in the various RE-doped systems at different temperatures as a function of ε in FIG. 8. It can be seen that the overall tendency is reasonable: with the increase of ε, the diffusivity of oxygen decreases, which means the better efficiency of reactive element. Although there are some fluctuations along with the linear trend, which is probably due to the statistical accuracy of MD calculations. At each temperature, the La and Hf elements have the largest ε values, the Zr has the smallest one, while Ce and Y are in between, which are in correspondence with our former evaluation of the efficiency of reactive element in view of diffusivity data. But compared to the diffusivity data, the parameter ε is much easier to calculate and more feasible to guide the selection of doping elements in practical applications.

5. Summary

The effects of doping reactive elements Ce, Hf, La, Y and Zr on the local structure and ionic diffusivities in liquid Cr_2O_3 have been investigated by the AIMD simulations. The short range order in both pure and doped liquid Cr_2O_3 mainly consists of the icosahedral 15*lm*, the crystal-like 14*lm* and 16*lm* bond pairs. The results show that minor addition of REs does not change the local geometric structure of liquid chromia significantly. Both the pair correlation functions and mean residence time indicate the same sequence of bonding strength as Hf-O>Zr-O>(Ce,Y)-O>La-O. The self-diffusion coefficients of Cr and O in liquid Cr_2O_3 are evaluated, and it is observed that O diffuse faster than Cr. The Hf and La are the most efficient elements in retarding the diffusion of Cr and O, the Ce and Y are the secondarily efficient ones and the Zr is the least efficient one. The efficiency of reactive elements on retarding the diffusivities of Cr and O ions is discussed in terms of ionic size, bonding strength and ionic weight. It is observed that no sole factor could be responsible for the relative efficiency of reactive elements, and the ionic size and the bonding strength exhibit a competing influence on the efficiency of reactive element. A novel parameter combining the contributions of all the three factors has been suggested.

Acknowledgement

This work was financially supported by the National Energy Technology Laboratory (under the grant No. 2010-SC-RES-30033026 and the RES contract DE-FE00400 in Turbines) in the Unites States. First-principles calculations were carried out on the LION clusters at the Pennsylvania State University supported by the Materials Simulation Center and the Research Computing and Cyber infrastructure unit at the Pennsylvania State University and the CyberStar cluster funded by NSF through grant OCI-0821527.

Captions of Figures

FIG. 1. (Color online) Pair correlation functions at the temperatures investigated for the pure and RE-doped liquid Cr_2O_3. (For clarity, pair correlation function curves for distinct systems have been shifted by 1.0 vertically from lower to upper)

FIG. 2. (Color online) Variation of the proportions of various bond pairs with temperature for pure (solid lines and closed symbols) and Hf-doped liquid Cr_2O_3 (dash lines and open symbols)

FIG. 3. (Color online) Mean square displacements of Cr and O ions at 2705 K as a function of time for the pure and RE-doped systems. (The symbols are shown to clarify the curves)

FIG. 4. (Color online) Velocity autocorrelation functions of Cr and O ions vs. time at 2705 K for the pure (solid line) and Hf-doped liquid Cr_2O_3 (dash line)

FIG. 5. (Color online) Ratios of D_{Cr} (D_{O}) in the RE-doped liquid chromia with those in pure liquid chromia from the mean square displacement (MSD) and velocity autocorrelation function (VACF) methods respectively at (a) 4000 K, (b) 3300 K, (c) 2705 K. (d) The Arrhenius plots showing the temperature dependence of the O diffusivities. (The lines are drawn to guide the eye)

FIG. 6. (Color online) Mean residence time of O ions in the first neighboring range around (a) Cr and (b) RE (RE = Ce, Hf, La, Y, Zr) ions

FIG. 7. (Color online) The empirical relationship of bonding strength with the valence, coordination number and ionic radius of cations at the temperature of 2705 K

FIG. 8. (Color online) Diffusivity of oxygen vs. the effective parameter at different temperatures (The lines are drawn to guide the eye)

Captions of Tables

Table I. First peak positions of pair correlation function curves r_{max}, the coordination numbers $N_{\alpha\beta}$ and the cutoff values r_{cut}

Table II. Diffusivities of Cr and O ions in pure and RE-doped liquid chromia at the temperatures investigated derived by MSD and VACF (in bracket) methods, unit: 10^{-8} m^2/s. The statistical errors are also shown for both methods.

Table III. Comparison of cation radius, cation weight, melting temperature T_m (K), enthalpy of formation ΔH_f and enthalpy of melting ΔH_m (kJ/mole of metallic atoms) of various oxides

Fang et al, FIG. 1

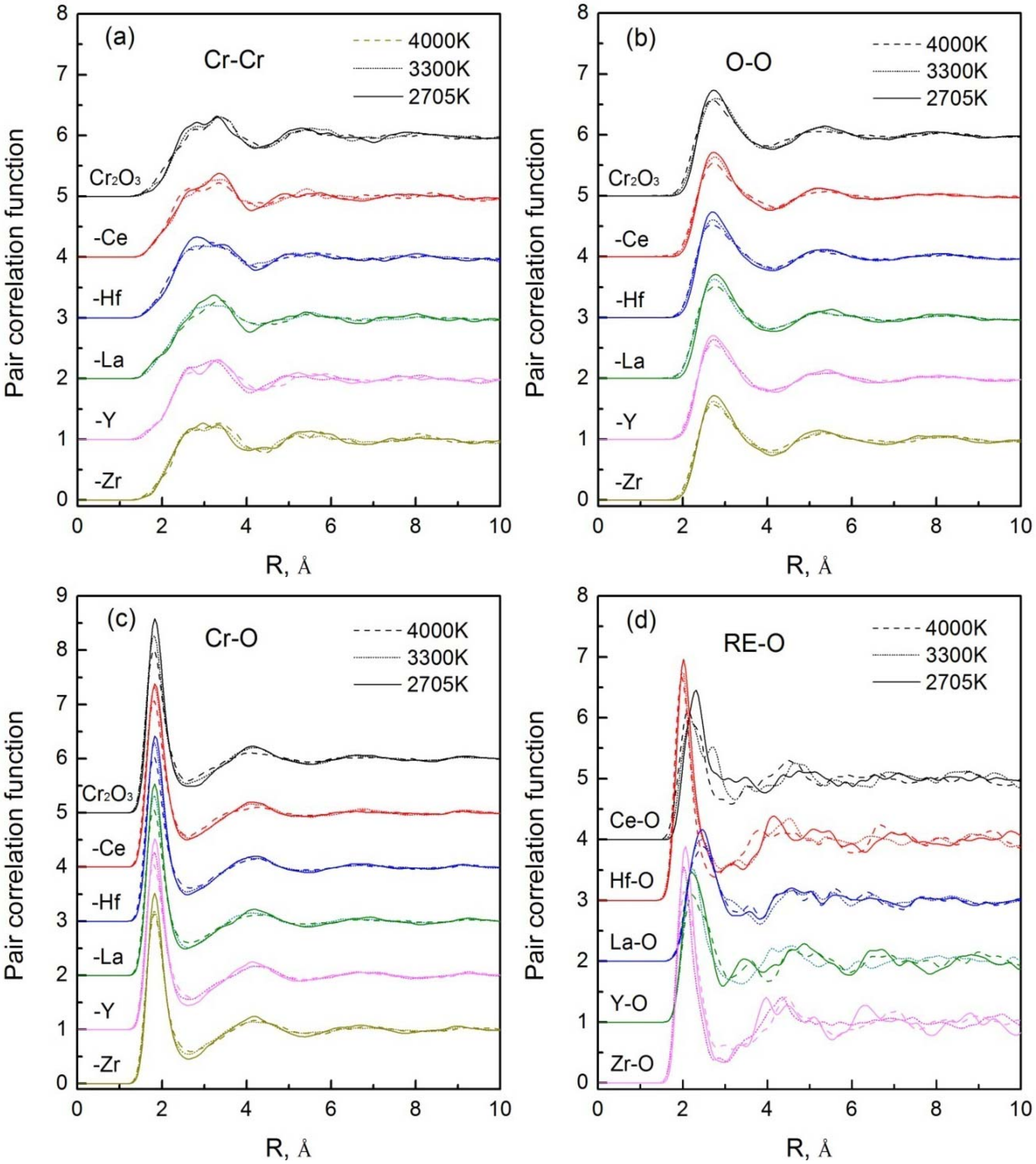

Fang et al, FIG. 2

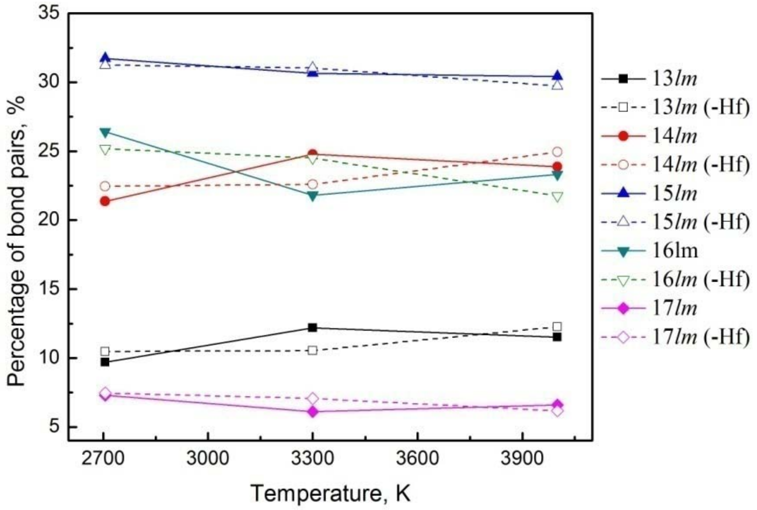

Fang et al, FIG. 3

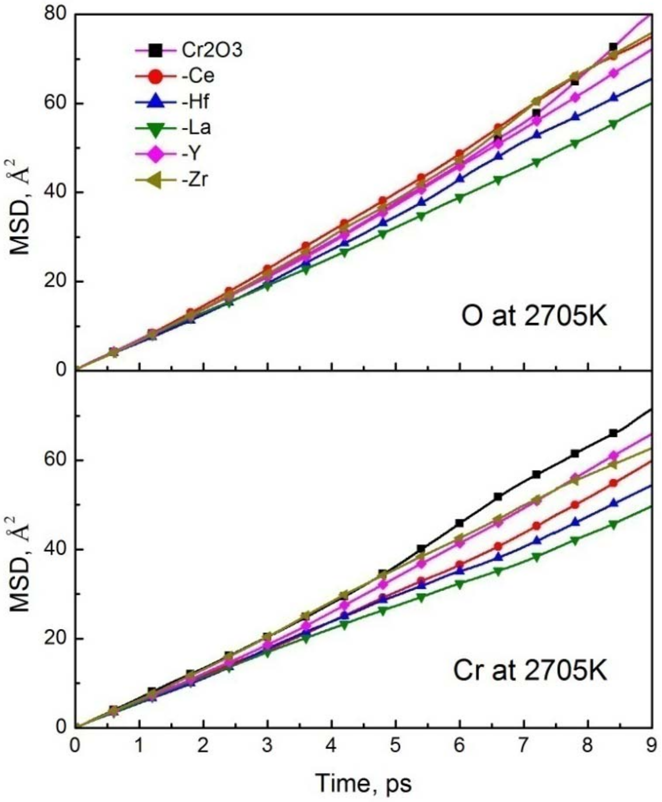

Fang et al, FIG. 4

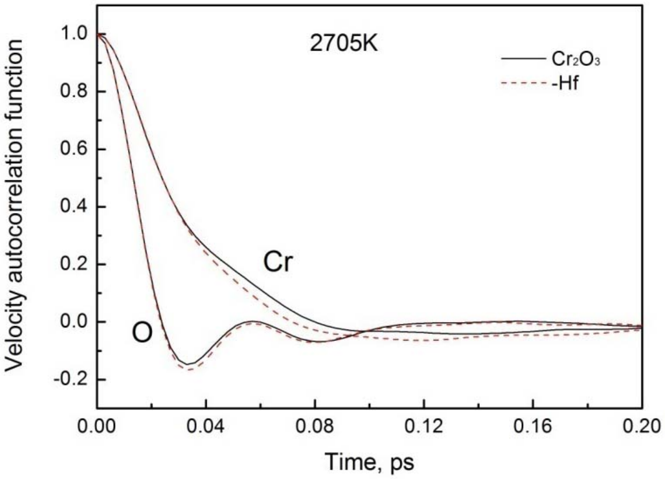

Fang et al, FIG. 5

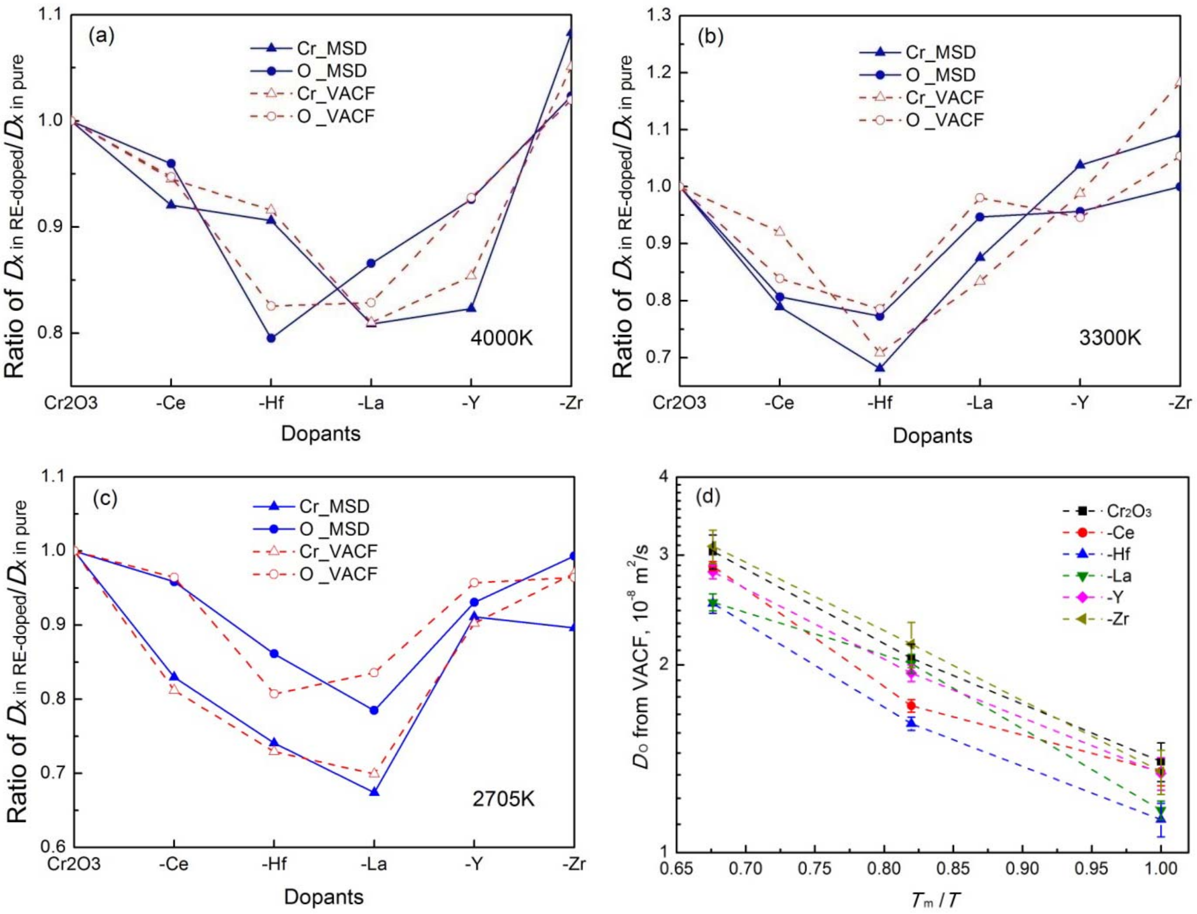

Fang et al, FIG. 6

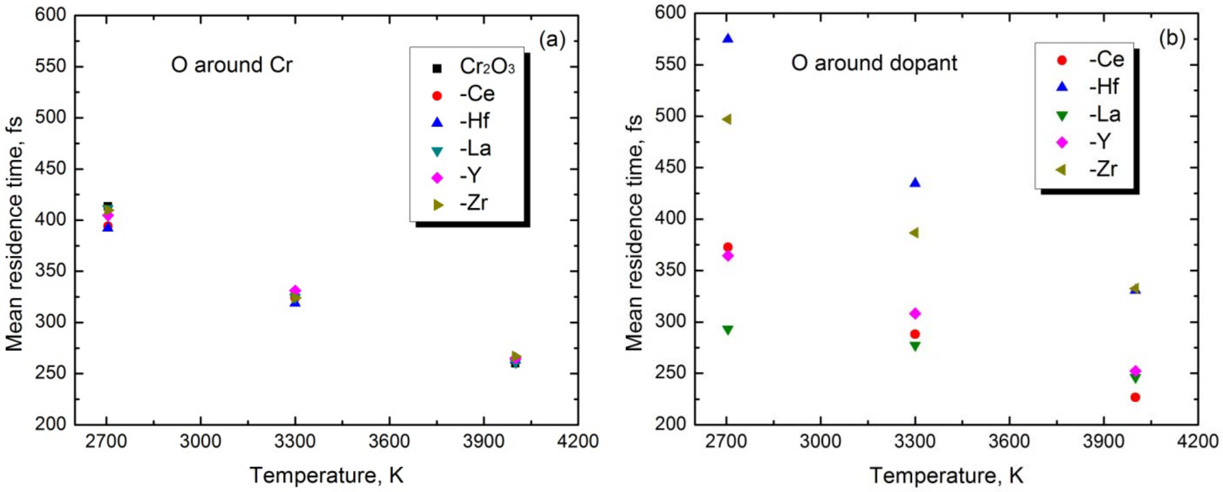

Fang et al, FIG. 7

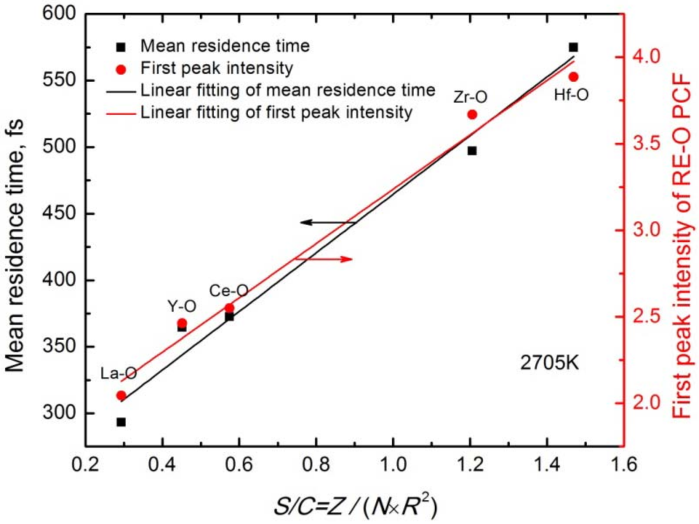

Fang et al, FIG. 8

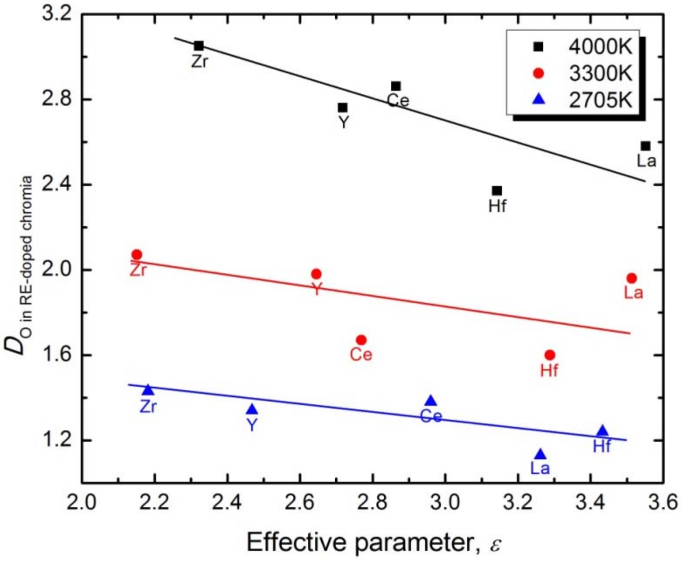

Fang et al, Table

	State	Cr-Cr*	O-O*	Cr-O*	Ce-O	Hf-O	La-O	Y-O	Zr-O
r_{max} /Å	4000K	2.78,3.33	2.68	1.83	2.13	2.00	2.48	2.23	2.03
	3300K	2.88,3.33	2.78	1.83	2.18	1.98	2.38	2.23	2.03
	2705K	2.83,3.33	2.73	1.83	2.33	2.03	2.43	2.23	2.08
	crystal	2.89,3.42	2.62	1.96	—	—	—	—	—
$N_{\alpha\beta}$	4000K	11.2	12.9	4.4	5.8	5.9	10.4	7.7	6.2
	3300K	10.9	12.8	4.4	7.2	6.2	10.6	7.5	5.6
	2705K	11.1	13.2	4.6	6.9	5.4	9.6	8.2	6.4
	crystal	14	16	6	—	—	—	—	—
r_{cut} /Å		4.43	4.03	2.63	3.18	2.88	3.78	3.38	2.98

* indicates pure Cr_2O_3 without dopants

Fang et al, Table

		Cr_2O_3	-Ce	-Hf	-La	-Y	-Zr
D_{Cr}	4000K	2.77±0.33 (2.74±0.17)	2.55±0.17 (2.59±0.16)	2.51±0.29 (2.51±0.07)	2.24±0.22 (2.22±0.13)	2.28±0.29 (2.34±0.06)	3.00±0.34 (2.88±0.17)
	3300K	1.85±0.35 (1.75±0.05)	1.46±0.19 (1.61±0.06)	1.26±0.16 (1.24±0.06)	1.62±0.15 (1.46±0.06)	1.92±0.30 (1.73±0.05)	2.02±0.23 (2.07±0.15)
	2705K	1.35±0.19 (1.33±0.08)	1.12±0.16 (1.08±0.07)	1.00±0.10 (0.97±0.06)	0.91±0.09 (0.93±0.04)	1.23±0.15 (1.20±0.07)	1.21±0.09 (1.29±0.07)
D_O	4000K	2.98±0.27 (3.04±0.19)	2.86±0.12 (2.88±0.05)	2.37±0.16 (2.51±0.09)	2.58±0.41 (2.52±0.08)	2.76±0.15 (2.82±0.07)	3.05±0.24 (3.10±0.19)
	3300K	2.07±0.38 (2.05±0.11)	1.67±0.10 (1.72±0.04)	1.60±0.09 (1.61±0.04)	1.96±0.15 (2.01±0.07)	1.98±0.11 (1.94±0.06)	2.07±0.20 (2.16±0.18)
	2705K	1.44±0.34 (1.40±0.10)	1.38±0.16 (1.35±0.07)	1.24±0.15 (1.13±0.07)	1.13±0.08 (1.17±0.04)	1.34±0.14 (1.34±0.08)	1.43±0.25 (1.35±0.11)

Fang et al, Table III

	Cation radius [a]	Cation weight	T_m [b]	ΔH_f [b]	ΔH_m [b]
HfO_2	0.71	178.5	2903	-1116	126
ZrO_2	0.72	91.2	2720	-1100	111.4
CeO_2	0.87	140.1	2753	-1090	80.1
Y_2O_3	0.9	88.9	2644	-953	67.5
La_2O_3	1.032	138.9	2444	-898	91.25
Cr_2O_3	0.615	52.0	2705	-570	62.5

[a] Data from Ref. 34

[b] Data from Ref. 42

References

[1] J. E. Hammer, S. J. Laney, R. W. Jackson, K. Coyne, F. S. Pettit, and G. H. Meier, Oxid. Met. **67**, 1 (2007).

[2] L. Ramanathan, M. Pillis, and S. Fernandes, J. Mater. Sci. **43**, 530 (2008).

[3] H. S. Seo, G. X. Jin, J. H. Jun, D. H. Kim, and K. Y. Kim, J. Power Sources **178**, 1 (2008).

[4] J. M. N'gandu-Muamba and R. Streiff, J. Phys. IV **3**, 281 (1993).

[5] J. Stringer, Mater. Sci. Eng. A **120**, 129 (1989).

[6] P. Y. Hou and J. Stringer, Mater. Sci. Eng. A **202**, 1 (1995).

[7] B. A. Pint, in *Proc. John Stringer Symposium on High Temperature Corrosion* (ASM International, Materials Park, OH, 2003), p. 9.

[8] N. Shaigan, W. Qu, D. G. Ivey, and W. X. Chen, J. Power Sources **195**, 1529 (2010).

[9] A. Paul, J. A. Odriozola, M. A. San Miguel, J. Fernandez Sanz, and L. J. Alvarez, Acta Mater. **48**, 2951 (2000).

[10] S. Fontana, R. Amendola, S. Chevalier, P. Piccardo, G. Caboche, M. Viviani, R. Molins, and M. Sennour, J. Power Sources **171**, 652 (2007).

[11] E. A. Polman, T. Fransen, and P. J. Gellings, J. Phys.: Condens. Matter **1**, 4497 (1989).

[12] A. M. Huntz and S. C. Tsai, J. Mater. Sci. Lett. **13**, 821 (1994).

[13] S. C. Tsai, A. M. Huntz, and C. Dolin, Mater. Sci. Eng. A **212**, 6 (1996).

[14] P. Kansuwan and J. M. Rickman, J. Chem. Phys. **126**, 094707 (2007).

[15] D. Wolf, Curr. Opin. Solid State Mater. Sci. **5**, 435 (2001).

[16] H. Zhang, D. J. Srolovitz, J. F. Douglas, and J. A. Warren, Proc. Natl. Acad. Sci. **106**, 7735 (2009).

[17] S. J. Dillon, M. P. Harmer, and J. Luo, JOM **61**, 38 (2009).

[18] J. Luo, Crit. Rev. Solid State Mater. Sci. **32**, 67 (2007).

[19] X. Hui, H. Z. Fang, G. L. Chen, S. L. Shang, Y. Wang, and Z. K. Liu, Appl. Phys. Lett. **92** (2008).

[20] X. Hui, H. Z. Fang, G. L. Chen, S. L. Shang, Y. Wang, J. Y. Qin, and Z. K. Liu, Acta Mater. **57**, 376 (2009).

[21] H. Z. Fang, X. Hui, G. L. Chen, and Z. K. Liu, Appl. Phys. Lett. **94** (2009).

[22] H. Z. Fang, X. Hui, G. L. Chen, and Z. K. Liu, Phys. Lett. A **372**, 5831 (2008).

[23] H. W. Sheng, W. K. Luo, F. M. Alamgir, J. M. Bai, and E. Ma, Nature **439**, 419 (2006).

[24] G. Kresse and J. Furthmüller, Phys. Rev. B **54**, 11169 (1996).

[25] G. Kresse and J. Furthmüller, Comput. Mater. Sci. **6**, 15 (1996).

[26] G. Kresse and D. Joubert, Phys. Rev. B **59**, 1758 (1999).

[27] Y. Wang and J. P. Perdew, Phys. Rev. B **44**, 13298 (1991).

[28] S. Nosé, J. Chem. Phys. **81**, 9 (1984).

[29] H. J. Monkhorst and J. D. Pack, Phys. Rev. B **13**, 5188 (1976).

[30] G. V. Samsonov, *The Oxide Handbook* (IFI/Plenum, New York, 1973).

[31] M. P. Allen and D. J. Tildesley, *Computer Simulation of Liquids* (Oxford University Press, 1989).

[32] D. Frenkel and B. Smit, *Understanding Molecular Simulation : from algorithms to applications* (Academic Press, San Diego, 2002).

[33] E. L. Belokoneva and Y. K. Shcherbakova, Russ. J. Inorg. Chem. **48**, 861 (2003).

[34] R. Shannon, Acta Crystallogr. Sect. A **32**, 751 (1976).

[35] J. D. Honeycutt and H. C. Andersen, J. Phys. Chem. **91**, 4950 (1987).

[36] A. C. S. Sabioni, A. M. Huntz, J. Philibert, B. Lesage, and C. Monty, J. Mater. Sci. **27**, 4782 (1992).

[37] J. H. Park, W. E. King, and S. J. Rothman, J. Am. Ceram. Soc. **70**, 880 (1987).

[38] B. Burton and G. L. Reynolds, J. Mater. Sci. **13**, 219 (1978).

[39] D. E. Kim, S.-L. Shang, B. Gleeson, and Z.-K. Liu, in preparation (2011).

[40] C. M. Wang, G. S. Cargill, M. P. Harmer, H. M. Chan, and J. Cho, Acta Mater. **47**, 3411 (1999).

[41] J. Cho, H. M. Chan, M. P. Harmer, and J. M. Rickman, J. Am. Ceram. Soc **81**, 3001 (1998).

[42] Scientific Group Thermodata Europe (SGTE). *Thermodynamic Properties of Inorganic Materials*. (Springer-Verlag, Berlin, Heidelberg, 1999).

[43] X. P. Su, S. Yang, J. H. Wang, N. Y. Tang, F. C. Yin, Z. Li, and M. X. Zhao, J Phase Equilib Diff **31**, 333 (2010).

[44] H. M. Lu, G. Li, Y. F. Zhu, and Q. Jiang, J. Non-Cryst. Solids **352**, 2797 (2006).

[45] N. H. Nachtrieb, Ber Bunsen Phys Chem **80**, 678 (1976).

[46] L. Pauling, J. Am. Chem. Soc. **51**, 1010 (1929).

[47] I. D. Brown and R. D. Shannon, Acta Crystallogr. Sect. A **A 29**, 266 (1973).

[48] J. Ziolkowski, J. Solid State Chem. **57**, 269 (1985).